Heat Treatment and Surface Engineering

ISSN: 2578-7616 (Online) Journal homepage: www.tandfonline.com/journals/thts20

Thermal-reduction and -oxidation of iron oxide slags generated from rolling mill steel industry

J. Kargin, H. Sanchez Cornejo, Y. V. Konyukhov, A. S. Lileev, A. Kozlovskiy, J. Albino Aguiar, V. A. J. Silva, S. R. Celis Rojas, C. H. W. Barnes & L. De Los Santos Valladares

To cite this article: J. Kargin, H. Sanchez Cornejo, Y. V. Konyukhov, A. S. Lileev, A. Kozlovskiy, J. Albino Aguiar, V. A. J. Silva, S. R. Celis Rojas, C. H. W. Barnes & L. De Los Santos Valladares (2025) Thermal-reduction and -oxidation of iron oxide slags generated from rolling mill steel industry, Heat Treatment and Surface Engineering, 7:1, 2494356, DOI: 10.1080/25787616.2025.2494356

To link to this article: https://doi.org/10.1080/25787616.2025.2494356

HEAT TREATMENT AND SURFACE ENGINEERING
2025, VOL. 7, NO. 1, 2494356
https://doi.org/10.1080/25787616.2025.2494356

I·M3 Institute of Materials, Minerals & Mining
Taylor & Francis Taylor & Francis Group

Thermal-reduction and -oxidation of iron oxide slags generated from rolling mill steel industry

J. Kargin[a], H. Sanchez Cornejo[b], Y. V. Konyukhov[c], A. S. Lileev[c], A. Kozlovskiy[a], J. Albino Aguiar[d], V. A. J. Silva[d], S. R. Celis Rojas[e], C. H. W. Barnes[f] and L. De Los Santos Valladares [d,f]

[a]L.N. Gumilyov Eurasian National University, NPJSC, Astana, Kazakhstan; [b]Laboratorio de Cerámicos y Nanomateriales, Facultad de Ciencias Físicas, Universidad Nacional Mayor de San Marcos, Lima, Peru; [c]National University of Science and Technology, MISIS, Moscow, Russia; [d]Programa de Pós-Graduação em Ciências de Materiais, Centro de Ciências Exatas e da Natureza, Universidade Federal de Pernambuco, Recife, Brazil; [e]Facultad de Ingeniería, Universidad Nacional de Barranca, Barranca, Peru; [f]Cavendish Laboratory, Department of Physics, University of Cambridge, Cambridge, UK

ABSTRACT

Every year, thousands of tons of waste scales are produced during rolling mill steel processing worldwide. The scales are rich in hematite and magnetite, and different ways of reduction and oxidation have been proposed for recycling the iron oxides. Modern methods for removing and processing steel scales fall into three classes: mechanical, chemical, and electrochemical approaches. Each method has its advantages and disadvantages, and the choice of method depends on cost and users' need for the final product. The present work reports the reduction of the mill scales by their precipitation in a mixture of HCl and HNO_3 acids to form α-FeOOH nanopowder, followed by thermal oxidation in a hydrogen atmosphere at 400°C and 375°C. This approach combines chemical and physical processes and it is known as chemical metallurgical method. Sodium dodecyl sulphate is used as a surfactant to obtain Fe and Fe_3O_4 powders. X-ray diffraction analysis shows that thermal treatment results in the formation of γ-Fe_2O_3 phase. It also causes a transition from magnetite (Fe_3O_4) to γ-Fe_2O_3, with a preferential crystallite orientation of the γ-Fe_2O_3 phase to the (220) texture plane. Eventually, longer thermal treatment time increases the crystallite size for the γ-Fe_2O_3 phase and decreases it for the Fe_3O_4 phase.

ARTICLE HISTORY
Received 27 December 2024
Revised 1 April 2025
Accepted 11 April 2025

KEYWORDS
reduction of iron oxides; catalyst; thermal oxidation; rolling mill steel slag; Iron oxide slags

Introduction

The recycling of steel slags and rolling mill scales present environmental and economic challenges. Recent discussions emphasize the need for efficient, cost-effective methods to repurpose these industrial by-products. This reduces waste accumulation and promotes circular economy principles. Developing innovative approaches to recycle iron oxides minimizes environmental impact and allows for the sustainable production of advanced materials with tailored properties for various technologies. Globally, there is special attention ion recycling industrial waste, including productive, technogenic and radioactive types [1–3]. These wastes can pollute the environment and pose serious risks to human health. Since recycling industrial waste requires effective and affordable methods, several approaches have emerged [4–8]. These methods show innovative, efficiency and low cost.

In the case of the steel industry, the novel technologies for producing advanced materials from steel slags involve preliminary treatments such as grinding,pressing, bathing, vitrification, and annealing. These procedures occur under different atmospheric conditions and temperature [9–15].

Since steel is the main product of ferrous metallurgy in the world due to its ability to efficiently produce a wide range of products with improved mechanical properties, its recycling has been turned very important [8,11,13,16]. Rolling mill steel production can create a wide range of steel products with enhanced mechanical properties. This process involves passing steel through rollers to reduce thickness, improve uniformity, and achieve desired shapes. One by-product of steelmaking is rolled scales, which come from mechanically cleaning hot-rolled steel strips. During the rolling process, scale slags are produced from the surface oxidation of steel at 800–1200°C. In a previous work, the authors have reported the morphological and structural characterization of the scales by X-ray diffraction (XRD), scanning electron microscope adapted with an energy dispersive X-ray spectrometer (SEM-EDX), magnetometry and Mössbauer

CONTACT J. Kargin kargin_db@enu.kz L.N. Gumilyov Eurasian National University, NPJSC, Astana, 010000, Kazakhstan; L. De Los Santos Valladares ld301@cam.ac.uk Cavendish Laboratory, Department of Physics, University of Cambridge, J.J. Thomson Ave., Cambridge CB3 0HE, UK
Supplemental data for this article can be accessed online at https://doi.org/10.1080/25787616.2025.2494356.

Spectroscopy [4]. The results indicated that the raw sample consists of α-Fe_2O_3 (hematite) and Fe_3O_4 (magnetite) and the scales completely oxidize to α-Fe_2O_3 after annealing at 1000°C. Annealing at 250–400°C results in a mixture of magnetite, maghemite and hematite [14,17]. Single hematite phase in the form of hollow microspheres is obtained after annealing at 550°C and 600°C [14,17]. The crystallization and crystal size of the hematite shells grow with higher annealing temperatures [14,17].

In work [18], the authors of this study investigated the influence of thermal and thermomagnetic treatment on the magnetic properties of iron–cobalt oxides in compacted samples fabricated by powder metallurgy. In particular, X-ray diffraction analysis showed that annealing pressed samples of α-Fe (50%) + Fe_2O_3 (50%) at 250°C in air promotes the oxidation of α-Fe and FeO to magnetite (Fe_3O_4), while thermomagnetic treatment of the α-Fe (50%) + Fe_2O_3 (30%) + Co_3O_4 (20%) system does not improve its magnetic properties.

For magnetite, efficient industrial production relies on a suitable synthesis method, since its properties depend on the structure and synthesis process. Several methods for making maghemite (γ-Fe_2O_3) nanoparticles have been proposed. These include chemical precipitation from iron (II, III) chloride solutions [19], recycling wasted condensed milk cans [20], and creating a mixed-phase iron oxide (IO) and recycled polyamide (RPA) composite from textile waste [21]. In the case of maghemite (γ-Fe_2O_3) nanoparticles, the synthesis exhibits significant variations in terms of reaction mechanisms, particle morphology, microstructural characteristics, and magnetic properties, depending on the selection of precursor and process conditions.

The chemical precipitation method [19] involves the coprecipitation of iron (II, III) chlorides in an alkaline medium under controlled conditions, including external factors like ultrasound, inert gas bubbling, and heating at 70°C. This process created nanosized particles (∼10–25 nm) with a spherical shape with a solid solution of magnetite and maghemite. Ultrasound during precipitation accelerates Fe^{2+} oxidation, increasing the maghemite content. However, longer aging in the mother solution promotes particle agglomeration. Despite this method produces highly homogeneous nanopowders, it requires careful synthesis control, making it technically challenging.

In contrast, the acid leaching precipitation method [20] facilitates the transformation of waste iron-based materials into γ-Fe_2O_3 nanoparticles. This method involves several steps. First, iron is leached from waste condensed milk cans using hydrochloric acid at 80–90°C. Then NaOH is added to precipitate iron hydroxides at pH 12–14. After that the material is dried and calcined at 200–350°C. The obtained maghemite nanoparticles have a crystallite size of 27–52 nm and cubic spinel structure, confirmed by X-ray diffraction. The saturation magnetization (*M*s) reaches 54.94 emu/g, indicating strong ferrimagnetic behaviour. This method provides a sustainable alternative for recycling industrial iron waste into functional nanomaterials. However, the resulting particles have higher polydispersity due to differences in precursor composition and synthesis conditions.

A third approach [21] focuses on preparing iron oxide–polyamide nanocomposites by combining iron oxide nanoparticles with recycled textile-based polyamide (RPA). The resulting material contains mixed-phase iron oxides: 76.8 wt% maghemite and 23.2 wt % magnetite, as determined by Rietveld refinement. The nanoparticles have an average size of ∼14 nm. They exhibit ferrimagnetic and superparamagnetic behaviors, with saturation magnetization values of 21.81 emu/g at 5 K and 18.84 emu/g at 300 K. The presence of a polymeric matrix alters the anisotropy, which reduces the magnetic response compared to pure maghemite. This method efficiently integrates iron oxide nanoparticles into a polymeric composite. However, it has limitations such as lower magnetic saturation and presence of non-magnetic organic phases.

Some studies on the reduction and oxidation of steel slags are reported in the literature. About reduction, a novel carbothermal route for extracting iron from red mill scales and transforming it into ferro-aluminium alloys in the presence of alumina is reported in reference [22]. The study shows that red milling waste can produce iron aluminides (Fe–Al) alloys and various compositions. On the other hand, thermal annealing is the traditional technique for oxidizing metals. One of the main advantages of thermal oxidation is the prevention of internal stress. Stress can lead to a number of cutting defects which results in failure of the structure. An ordered structure increases the resistance to external forces. The duration of thermal treatment also affects conductive properties. Extended thermal annealing can cause irreversible changes in physical parameters [23,24]. In this context, it is also interesting to study the thermal oxidation processes of steel slags with annealing time, which provides useful information for posterior recycling of the waste materials. Moreover, studying the thermal reduction of steel slags, followed by thermal oxidation, could be useful to understand the structural properties and phase transformations occurring in the iron oxide components of the steel slags.

In this work, we examine the thermal reduction and oxidation of iron oxide waste scales obtained from the rolling mill steel industry. The reduction process and subsequent oxidation of the slags are described, and the products are analyzed by SEM and XRD. The resulting information could be helpful for potential

applications in steel recycling, catalysis, biomedicine and sensors. The novelty of this study lies in the use of rolling mill scale as a raw material for obtaining magnetite powder via a chemical–metallurgical method, which allows precise control over phase composition and particle size distribution. Unlike traditional methods, that rely on direct thermal or chemical treatments of iron oxides, our approach combines chemical precipitation with thermal processing. This ensures better purity and structural uniformity in the final magnetite and maghemite products. Additionally, the sequential thermal reduction and oxidation processes in the present work occur under controlled conditions. This provides new insights into phase transformations and microstructural evolution, contributing to optimize recycling strategies for industrial iron oxide waste. The use of sodium dodecyl sulphate as a surfactant in the reduction process enhances the functional properties of the synthesized Fe and Fe_3O_4 powders for applications in catalysis, magnetic materials, and environmental remediation.

Experimental

Initial samples

Figure 1(a) shows a schematic representation of the rolling mill steel manufacturing in a metallurgical plant. The scale formed on the surface of steel sheets during hot rolling ($T = 700–1200°C$) is called mill scale. The molten steel is initially poured from large bell furnaces into special molds (ingots or slabs) where it solidifies into a controllable shape. Then the hot solidifying slab undergoes an initial rolling or compression to reduce its thickness and make the material more homogeneous. Next, the slab passes through a series of rolling mills at high temperatures. This

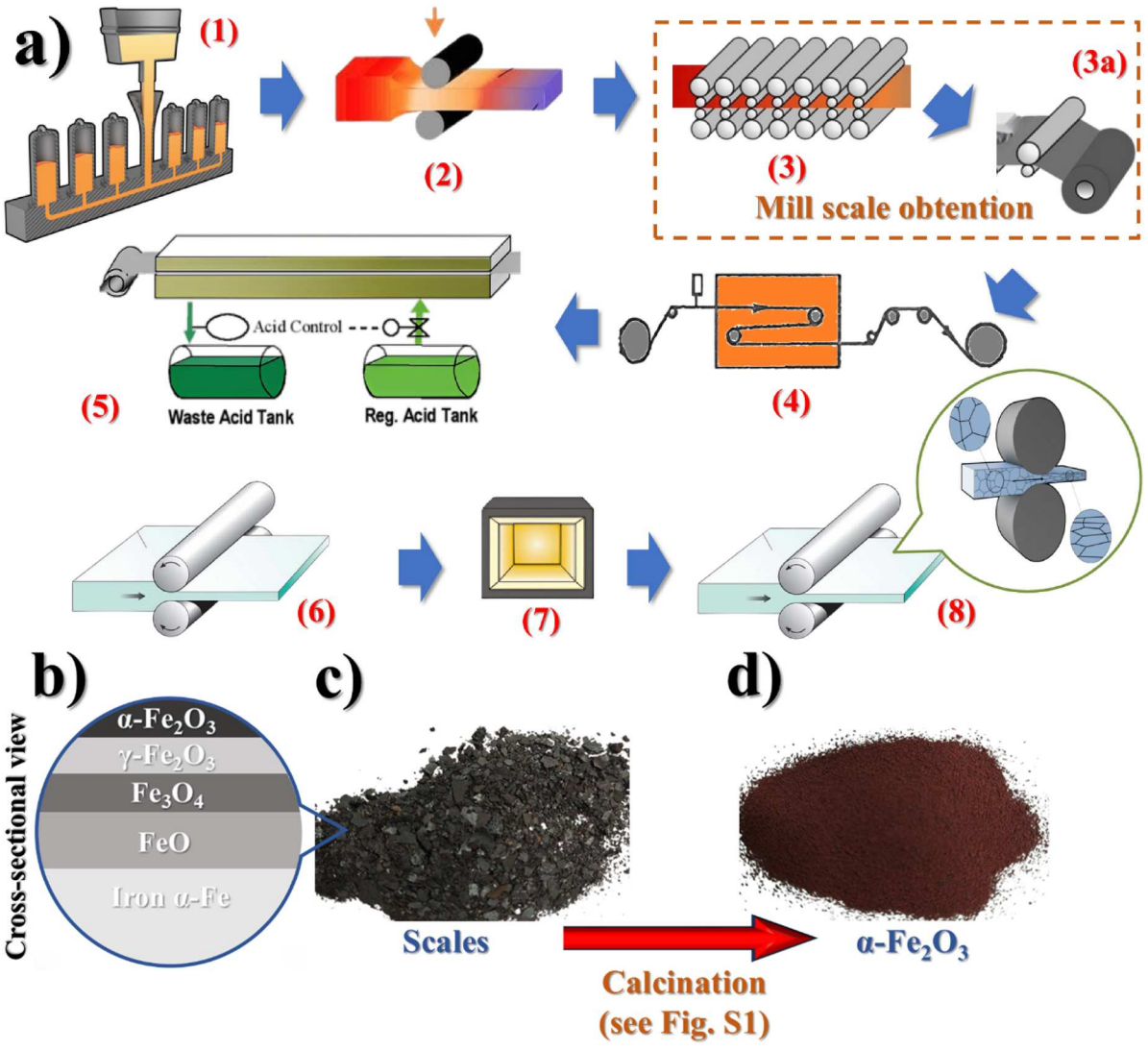

Figure 1. (a) Schematical representation of non-alloy cold-rolled steel production: (1) melting and casting of steel into ingots; (2) rolling of ingots to slabs; (3) hot rolling of slabs into strips; (3a) the scale breaker; (4) welding and coiling of strips to band; (5) pickling in hydrochloric acid; (6) the first cold rolling; (7) annealing of rolls in bell-type furnaces; and (8) the second cold rolling. (b) Schematical representation of the cross-sectional view of the surface of the formed steel. (c) Photo of the scales and (d) photo of the α-Fe_2O_3 component.

process further reduces the thickness of the steel and increases its length, forming a continuous steel strip. At stage 3a, the initial cleaning of the steel surface from scale occurs by passing the steel sheet through a scale breaker. This provides a cleaner steel surface for further processing as after hot rolling the steel surface is covered with scale (oxide layer). The mill scale obtained at this stage is called primary mill scale. Mill scale originates and grows on the surface of a steel sheet emerging from bell-type furnaces and consists of three phases. Figures 1(b) and (c) show the mill scales, which consist of a mixture of iron oxides, such as wüstite (FeO), magnetite (Fe_3O_4) and hematite (α-Fe_2O_3). Considering their cross section, mill scales are composites of different iron oxides (see Figure 1b). The outer layer of the scales is α-Fe_2O_3 and maghemite (γ-Fe_2O_3). A layer of magnetite is formed under it, and the wüstite (FeO) layer is closest to the metal. The thickness of these oxides depends on the processing temperature of the steel. At low temperatures (up to 570°C), magnetite and hematite predominate in the scale structure [25,26]. At temperatures above 570°C, the wüstite phase mainly grows [27].

The scaly particles are of varying thickness, consisting of iron oxides (2- and 3-valent). In terms of chemical composition, the scales are close to pure magnetite (65–72% Fe), and in terms of granulometric composition they represented mainly by a fraction of less than 0.2 mm [28]. The yield of mill scale is on average 1–3% by weight of the finished product. Mill scale should be removed before undergoing other technological processes like cold rolling, deposition of protective coatings, etc. The strip is descaled in two steps. First, the scale is separated from the surface of the steel strip using a scale breaker. This step is labelled as point 3a in Figure 1(a), in which the surface of the steel strip is cleaned by passing it through the scale breaker. The scale can be used, as an additive in ore raw materials, as it contains up to 70% iron, or, in the worst case, discarded as waste. The densest layer is the outer hematite, which creates difficulties in removal. Further cold rolling is possible only after the strip surface has been completely cleaned.

At stage 4 in Figure 1(a), the steel sheet undergoes additional cold rolling to improve its mechanical properties and dimensional accuracy. Then, at stage 5, the steel strip is passed through an acid bath (usually filled with hydrochloric or sulfuric acid) to remove the remaining scale or impurities from its surface, preparing it for further processing. The oxide layer that forms on the surface of the steel, as well as all surface impurities in the acid bath, dissolve and settle to the bottom of the bath. As discussed below, iron oxides are obtained during further processing of this acidic solution. At stage 6, the steel strip is rolled to the final thickness, achieving the desired dimensions and surface quality. The steel strip is then reheated in a furnace (annealed) to relieve the stresses caused by rolling, improve ductility, and reduce hardness at the Step 7. This process is called tempering. Finally, in Step 8, the strip undergoes a final rolling process to improve the surface characteristics and achieve the desired finish.

Reduction process

The schematic representation of the reduction process is shown in Figure S1 in the Supplemental Material. Prior to reduction, the scales were ground in a laboratory mortar for 3–5 min. This time was sufficient to obtain particles smaller than 1 mm. The next stage involved direct dissolution of the scales in HCl acid with different concentration under heating and stirring. The dissolution rate was very low, taking several days to completely dissolve the scales. On an industrial scale, the most common chemical method for removing scale from the strip surface consists of dissolving (etching) the iron oxides with a hydrochloric acid solution. Thus the original mill scale flakes were crushed and then dissolved in hydrochloric acid. In this case, the iron ions pass into solution, while the slag, consisting of insoluble impurities, remains in the precipitate. The reaction between the iron oxides hematite, magnetite and wüstite, which make up mill scale, with hydrochloric acid (HCl) leads to the formation of a solution of iron salts ($FeCl_2$ and $FeCl_3$) and water and the release of nitrogen dichloride gas (Cl_2). These processes are described by chemical reaction equations (1)–(3).

$$Fe_2O_3 + 6HCl \rightarrow 2FeCl_3 + 3H_2O; \quad (1)$$

$$Fe_3O_4 + 8HCl \rightarrow 2FeCl_3 + FeCl_2 + 4H_2O; \quad (2)$$

$$FeO + 2HCl \rightarrow FeCl_2 + H_2O; \quad (3)$$

The iron chloride formed during the interaction of HCl with scale dissolves well in water, which allows for the complete regeneration of all spent solutions without insoluble sediments. The resulting sludge from the scale residues precipitates and is removed during the washing of the baths and the strip surface. The spent etching solution is then fed as a spray through nozzles into the 600°C furnace. Evaporation of water leads to a concentration gradient in the droplets. The $FeCl_2$ remaining in the droplet is enriched in the outer shell. When the concentration of $FeCl_2$ reaches 63.6% in the shells, all of the $FeCl_2$ chloride binds as $FeCl_2{\cdot}4H_2O$ hydrate. This creates a solid layer of reduced permeability on the outer surface of the droplet [29]. Spray pyrolysis takes place in the furnace, in which iron chloride decomposes into finely dispersed oxide and hydrochloric

acid vapor according to pyrolysis reactions:

$$12FeCl_2 + 3O_2 \rightarrow 8FeCl_3 + 2Fe_2O_3 \downarrow \quad (4)$$

$$2FeCl_3 + 3H_2 \rightarrow 6HCl \uparrow + Fe_2O_3 \downarrow \quad (5)$$

Powdered hematite is separated from the exhaust gases in cyclones and is poured into the lower part of the reactor, and from there it goes into the bunker. Iron oxide is shipped in the form of powder or in the form of granules. At the metallurgical plant, it is usually used directly in the sintering plants [30,31]. Figure 1(d) shows the formed high purity hematite powder which is a valuable material for industrial products. The chemical–metallurgical method for the synthesis of hollow spherical hematite nanoparticles from mill scale is described in detail in the work [32]. The stages and conditions for obtaining the hematite and magnetite nanopowders from mill scale are shown in Figure S2 from Supplementary material.

To intensify the dissolution process, preliminary activation of the initial scale in a hydrogen flow was performed with the help of a Process Activation Setting (*Ustanovka Aktivacii Processov*, UAP-3, in Russian) magnetic mill, wherein a specially designed heating module with a stainless-steel flow reactor [33] (see Figure S3 in the supplementary information). The maximum value of the electromagnetic field induction is observed in the center of the reactor and is 0.16 T. The field rotation speed is 3200 rpm. The UAP-3 unit makes possible to recover samples of nanopowders under the application of an external rotating electromagnetic field [34]. Under the action of the rotating electromagnetic field, the ferromagnetic needles are driven into intensive motion, interacting with the treated material particles and with the walls of the working area. The total action of the factors results in a high activation level of the particle surface under treatment, and in an intense interaction

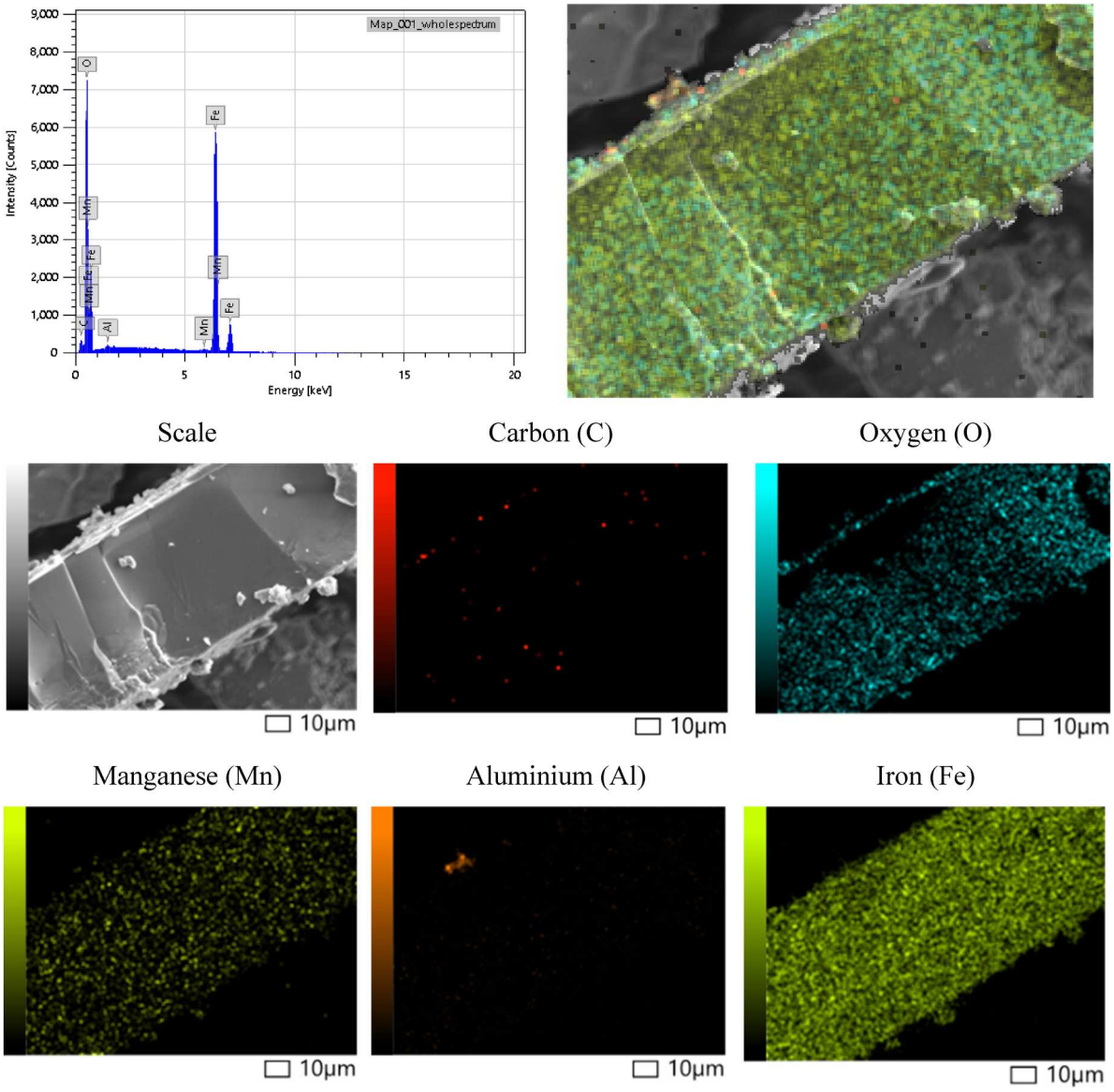

Figure. 2. Energy dispersive X-ray (EDX) analysis of the original mill scale. The pictures are the micrograph and EDX mapping for each detected element.

Table 1. Elemental composition of initial mill scales and iron oxide.

	Mill scale		Fe_2O_3	
Elements	Mass (%)	Atom (%)	Mass (%)	Atom (%)
Fe	66.22 ± 0.29	35.34 ± 0.16	77.55 ± 0.35	48.87 ± 0.22
O	28.86 ± 0.13	53.75 ± 0.25	18.62 ± 0.12	40.86 ± 0.27
C	4.14 ± 0.06	10.26 ± 0.14	3.42 ± 0.06	9.99 ± 0.17
Al	0.40 ± 0.03	0.21 ± 0.02	0.22 ± 0.03	0.28 ± 0.03
Mn	0.39 ± 0.03	0.43 ± 0.03	–	–
Total	100	100	100	100

between the particles and hydrogen. As the hydrogen source, an SAM-1 hydrogen generator (Russia) with a maximum capacity of 80 liter per hour was used. The hydrogen is previously passed through a drying system based on silica gel, which provided a moisture content of less than 10 ppm. The purity of the obtained hydrogen amounted to 99.99%, the output pressure ranging within 0.2–0.6 MPa. The scale was processed at 500°C for 15 min.

The dissolution of activated and partially reduced scale was carried out in a mixture of a special grade nitric acid HNO_3, GOST (State Standard) 11125–11184 (65–68 wt%) and a pure grade hydrochloric acid HCl, GOST (State Standard) 3118–3177 (32–35 wt%) taken at a volume ratio of 1:3 according to the technique presented in [35]. The duration time of complete dissolution did not exceed 1 h. The resulting solution was diluted with water to an iron salt concentration of about 5 wt%. The iron hydroxide precipitation was carried out using a NANOCHEM automatic laboratory reactor for obtaining nanosized materials from solutions. The installation involved a glass chemical reactor, Heidolph Pumpdrive 5201 pumps, a METTLER TOLEDO MP230 pH meter, a LAUDA E 300 thermostat, and a Heidolph RZR 2051 electric stirrer. The precipitation was performed using a 10% alkali solution at a constant pH value (pH 10). After the precipitation, it was filtered using a Buchner funnel and washed with distilled water. The precipitates were dried in an oven at a temperature of 80°C during 8 h.

Thermal oxidation

The iron hydroxide (FeOOH) obtained by reduction in hydrogen was used to study the effect of annealing time on the structural properties. The thermal oxidation of FeOOH was performed in two ways. In the first case, the obtained α-FeOOH was calcined in air at 200°C for 2 h in an SNOL 3/12 muffle furnace to obtained hematite nanopowder (see Figure S2). During this process, α-FeOOH is thermally decomposed at 200°C by the reaction:

$$2FeOOH \rightarrow Fe_2O_3 + H_2O, \quad (6)$$

In the second case, magnetite nanopowders (Fe_3O_4) were prepared by the reduction of the iron hydroxide (FeOOH) in a hydrogen current at 375°C in a Nabertherm RSR 120/750/11 tube furnace (see Figure S1), according to the following reaction:

$$3FeOOH + H_2 \rightarrow Fe_3O_4 + 2H_2O \quad (7)$$

The main method of γ-Fe_2O_3 is based on a controlled oxidation process of Fe_3O_4, which ensures the accumulation of cation vacancies in the structure and the formation of the γ-Fe_2O_3 phase:

$$2Fe_3O_4 + {}^1/_2O_2 \rightarrow 3\gamma - Fe_2O_3 \quad (8)$$

In this context, the process of obtaining γ-Fe_2O_3 from Fe_3O_4 has been performed by thermal treatment at

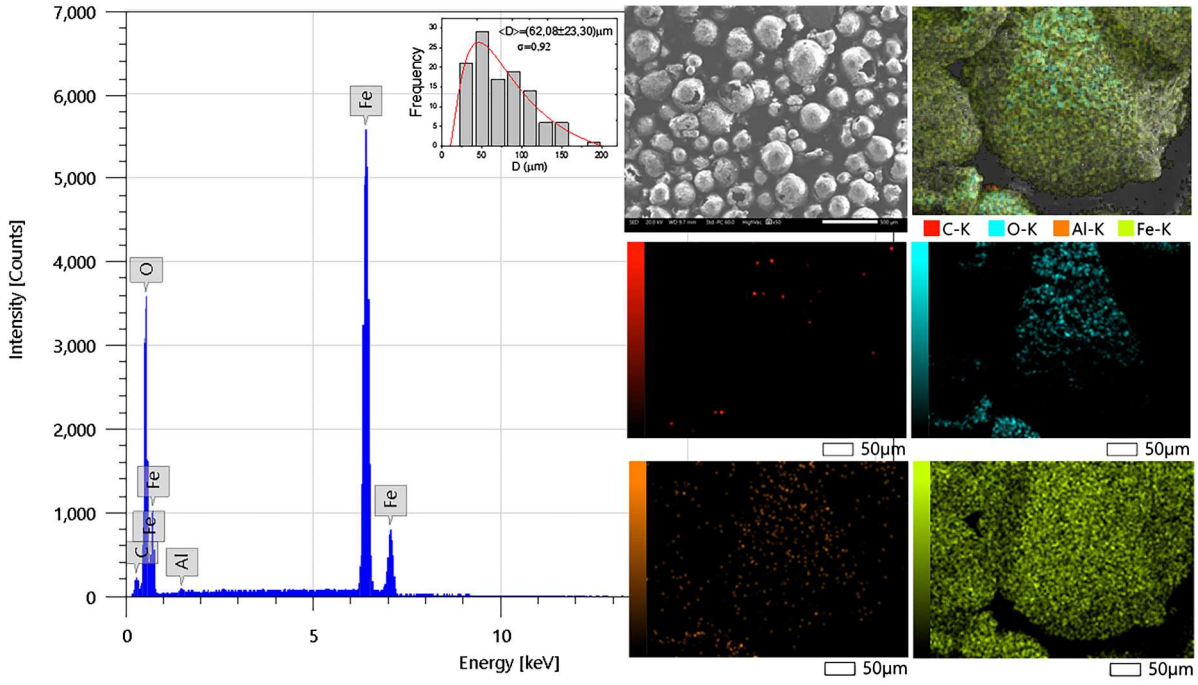

Figure. 3. Scanning electron micrograph and EDX analysis of the hollow microspheres.

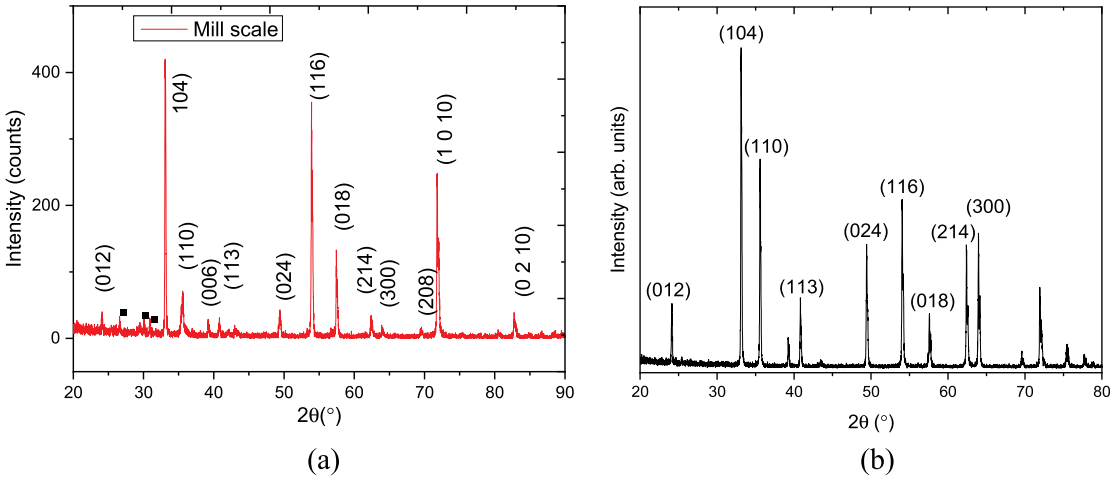

Figure 4. XRD data: (a) of iron oxide waste scales obtained by rolling mill steel industry and (b) XRD for red oxide powder α-Fe_2O_3.

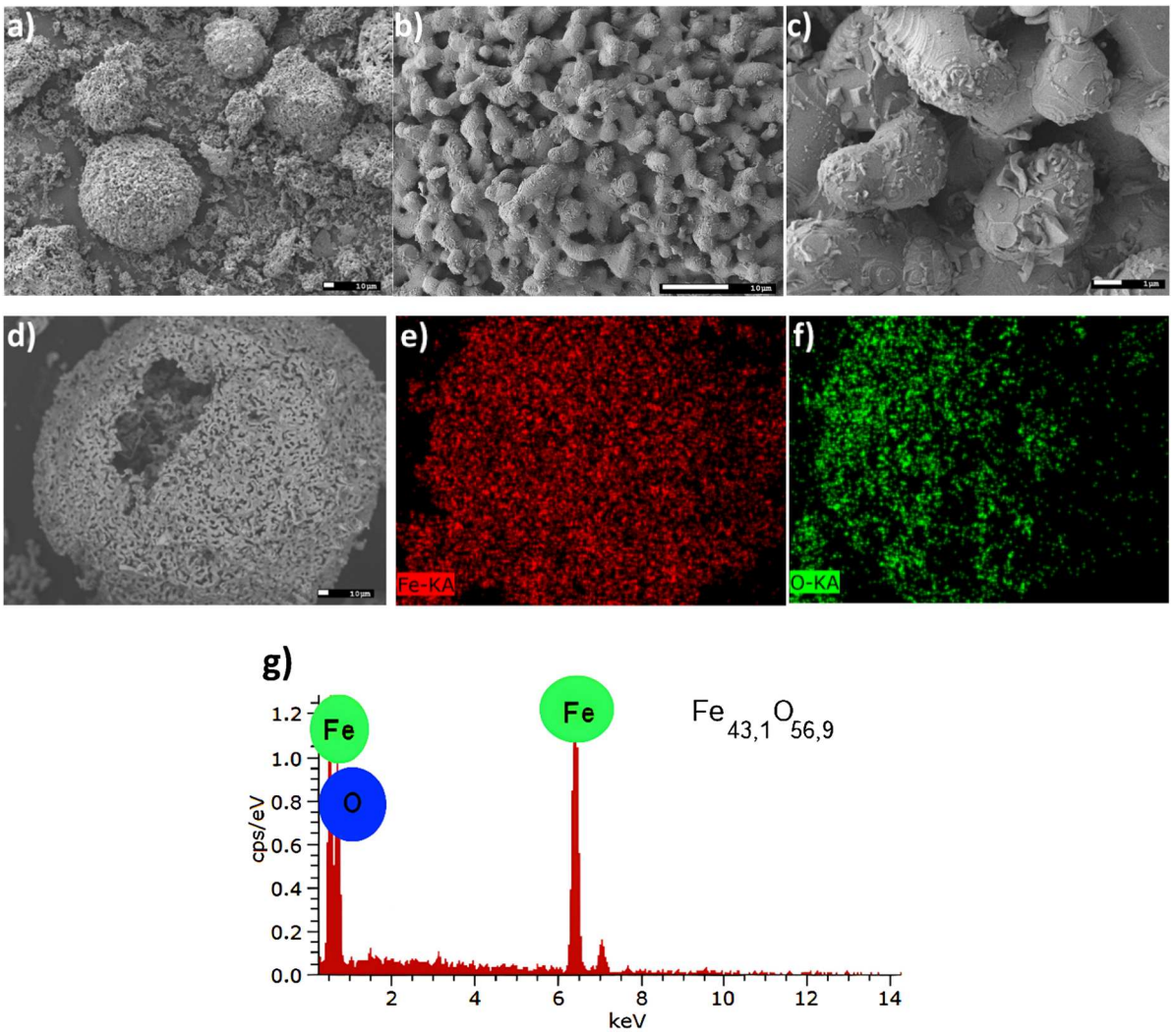

Figure 5. SEM images morphology reduced ultrafine Fe_3O_4 powder with different zoom (a–c) and its EDS spectrum (d–g).

300°C in the oxygen-containing atmosphere in a time range from 30 to 150 min.

Measurements

The morphological characterization and the element composition of the samples were obtained by using a Hitachi TM3030 scanning electron microscope (SEM) with the Bruker XFlash MIN SVE microanalysis system at the accelerating voltage of 15 kV. X-ray diffraction (XRD) analyses were performed with the help of a D8 ADVANCE ECO diffractometer using a X-ray tube radiation with a Cu anode and a graphite

Table 2. Comparison between results of reduction products in the present work and those obtained by other authors.

Synthesis method	Morphological features	Particle size	Main phases in the product	Magnetic properties	References
Chemical precipitation from aqueous solutions of iron (II, III) chlorides $FeCl_2 + 2FeCl_3 + 8NH_4OH \rightarrow Fe_3O_4 + 8NH_4Cl + 4H_2O$ Following ultrasonic agitation, results on the oxidation of magnetite to maghemite: $Fe_3O_4 + \frac{1}{4}O_2 + \frac{1}{2}H_2O \rightarrow 3\gamma - Fe_2O_3 + 2H^+$	Spherical nanoparticles (under ultrasonic agitation); needle particles (without ultrasonic agitation)	10–25 nm	Fe_3O_4 and γ-Fe_2O_3	Not specified	[19]
Acid leaching of iron-containing waste followed by thermal treatment $Fe - chips + 2HCl \overset{80^\circ C-90^\circ C}{\rightarrow} FeCl_2 + \uparrow H_2$ $FeCl_2 + NaOH \rightarrow Fe(OH)_2 \downarrow + NaCl$ $Fe(OH)_2 + Fe(OH)_3 \overset{300^\circ C}{\rightarrow} \gamma - Fe_2O_3$	Porous, agglomerated iron oxide surface	27–52 nm	γ-Fe_2O_3	Ferrimagnetic particles with saturation magnetization of 54.94 emu/g	[20]
Synthesis of an iron oxide composite with recycled polyamide from textile waste	Porous, agglomerated iron oxide surface	14 nm	Fe_3O_4 (23.2%) and γ-Fe_2O_3 (76.8%)	Saturation magnetization of 21.81 emu/g at 5 K and 18.84 emu/g at 300 K	[21]
Two steps for obtaining maghemite. On the first step we received magnetite nanopowders (Fe_3O_4) were prepared by reduction of the iron hydroxide (FeOOH): $3FeOOH + H_2 \overset{375^\circ C}{\rightarrow} Fe_3O_4 + 2H_2O$ The second stage is based on a controlled oxidation process of Fe3O4 during 30-150 min for synthesizing γ-Fe2O3: $2Fe_3O_4 + \frac{1}{2}O_2 \overset{300^\circ C}{\rightarrow} 3\gamma - Fe_2O_3$	The morphological transformations include coalescence, sintering, particle flattening, grain growth, increased porosity, and surface smoothing	42 nm	γ-Fe_2O_3	Not specified	This work

monochromator. The tube operation mode was 40 kV, 25 mA. The XRD patterns were recorded in the angular range of 10–90° (2θ) with 0.02° (2θ) step.

The lattice parameters were determined using the Nelson–Taylor extrapolation function:

$$a = f\left[\frac{1}{2}\left(\frac{\cos^2\theta}{\sin\theta} + \frac{\cos\theta}{\theta}\right)\right], \quad (9)$$

This method involves plotting the lattice parameter a against a specific function f of the diffraction angle to minimize systematic errors [36,37]. The value and error in determining the parameter a are evaluated by linear extrapolation of this function to the zero-argument value ($\theta = 90°$).

The average crystallite size D was evaluated by the Scherer equation:

$$D = \frac{k\lambda}{\beta\cos\theta}, \quad (10)$$

where $k = 0.9$ is the dimensionless particle shape factor (Scherer constant), $\lambda = 1.54$ Å is the X-ray radiation wavelength, β is the half-width of the reflex at half-height (FWHM), and θ is the diffraction angle (Bragg angle).

Results and discussion

Characteristics of the initial waste scales

Figure 2 shows the micrographs obtained by electron microscopy of the original mill scales. According to the figure, the scales have lamellar shapes of different sizes, ranging from millimeters to several centimeters. They are flat and spread without sticking together. They have thickness of the order 100–150 microns. It is also noted that the scales are composed of grains with planar fractured faces. According to the SEM micrograph of the scale, the faces of the grains are smooth suggesting good crystallinity although the grain boundary is not appreciable.

Figure 2 also shows the results of mapping and energy dispersive analysis of the original mill scale. The EDX mapping spectra for the mill scales shows that the main elemental components are Fe and O, suggesting the presence of iron oxides as main mineralogical phases. Some spots of Mn are spread over the samples. Table 1 lists the quantification of the main elements obtained by EDX. Manganese may proceed for the non-reacted manganese oxides added during the steelmaking process from ores [34]. The presence of carbon atoms is associated with its presence in the steel composition. The presence of aluminum atoms can be explained by the fact that some steel grades initially contain aluminum impurities to achieve specific properties such as improved grain structure, corrosion resistance, heat resistance and improved magnetic properties.

Figure 3 shows the microstructure of hollow microspheres obtained by spray annealing according to the reaction (6). The XRD analysis below show that the particles are made of α-Fe_2O_3 (hematite). The SEM micrograph shows that the particles are in an aggregated condition. The particles of α-Fe_2O_3 have a

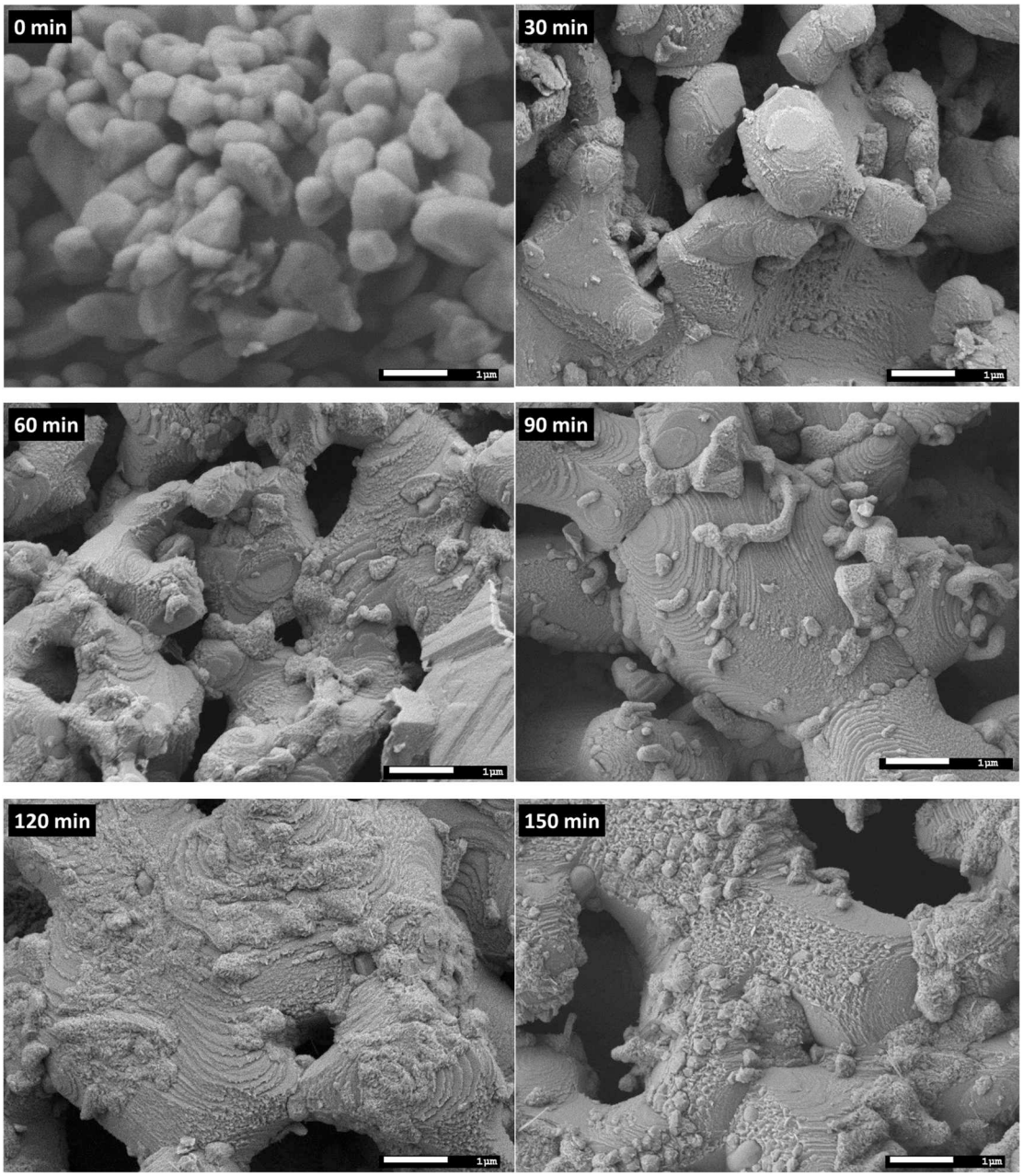

Figure 6. SEM images of powder (Fe_3O_4) surface morphology changes during annealing powder at 300°C for 30, 60, 90, 120, and 150 min.

predominantly spherical shape with an average size of particles (62 ± 23.3) µm. However, larger particles (up to 200 µm) can also be found.

Analysis of morphological data from Figure 3 showed that the hematite powder obtained by the above described chemical–metallurgical method from rolled mill scale is hollow microspheres with an average size of about 62 µm. The data of energy dispersive analysis confirm that the chemical composition of the obtained powder corresponds to hematite.

Table 1 shows a comparison of the elemental composition of rolled scales and hematite microparticles synthesized from it by the above chemical–metallurgical method. The mill scales contain impurity metals (manganese, aluminum), as well as carbon atoms. A large (4.14% by mass) amount of carbon in the initial scale is a consequence of the use of oil based on hydrocarbon mixtures to facilitate the hot rolling process in production. At the same time, during the synthesis of hematite from mill scale, the proportion of impurity elements decreases. The mass fraction of carbon is reduced by 17.3%, aluminum is reduced by 45%, and manganese is completely removed.

Figure 4(a) shows the X-ray diffraction pattern of the collected mill flakes. From these data, the main phase of the mill scale is α-Fe_2O_3 (hematite). Small reflection peaks between 25° and 33°, indicated by bold squares, are also detected, which may be related to some impurities according to the EDX results above. The X-ray diffraction pattern obtained (Figure 4b) reveals characteristic peaks on polycrystalline objects synthesized from rolled scale. Analysis of the peaks in the

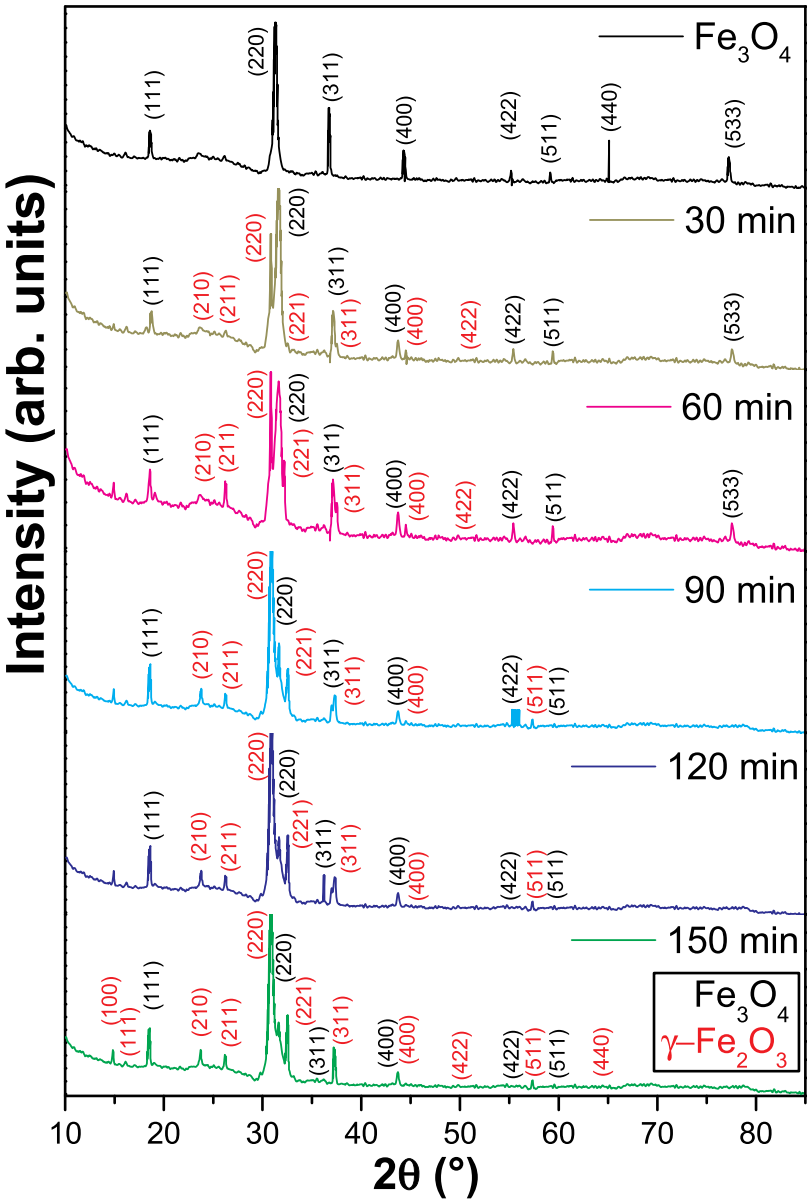

Figure 7. XRD pattern of the initial waste iron oxides coming from the rolling mill reduced powder (Fe_3O_4) and after annealing at 300°C for 30, 60, 90, 120, and 150 min.

diffraction pattern of the obtained powder from rolled scale showed the presence of a phase characteristic of iron oxide α-Fe_2O_3.

Analysis of the reduced samples

Figure 5 shows the SEM images of reduced Fe_3O_4 ultrafine powder obtained according to the reaction (7). It is seen that the Fe_3O_4 magnetite powder is spherical microparticles consisting of rhombic and cubic nanoparticles with an average size of 100 nm or less. Obviously, this spherical shape of hematite microparticles is due to the conditions of their synthesis by hydrogen reduction.

Energy dispersive X-ray spectroscopy (EDS) and X-ray diffraction (XRD) analysis were used to determine the structural, phase and elemental composition of the samples. Figures 5(e) and (f) show the EDS mapping and energy dispersive spectrum of the initial magnetite powder. Analysis of the EDS spectrum showed that the atomic ratio of elements before the process of thermal annealing was Fe – 43.1%, O – 56.9%, which corresponds to the iron oxides Fe_3O_4, γ-Fe_2O_3, or FeO, the oxidation degree of iron +2; +3, oxygen −2 in this compound. Table 2 compares the results of the reduction obtained in the present work with those obtained by other authors.

Table 3. Results of EDA analysis of the oxidized samples.

	Atomic ratio		
Annealing time (min)	Fe	O	Stoichiometric ratio
0	43.1	56.9	Fe_3O_4
30	42.5	57.5	Fe_3O_4
60	41.1	58.9	Fe_3O_4, Fe_2O_3
90	40.9	59.1	Fe_2O_3
120	40.5	59.5	Fe_2O_3
150	40.4	59.6	Fe_2O_3

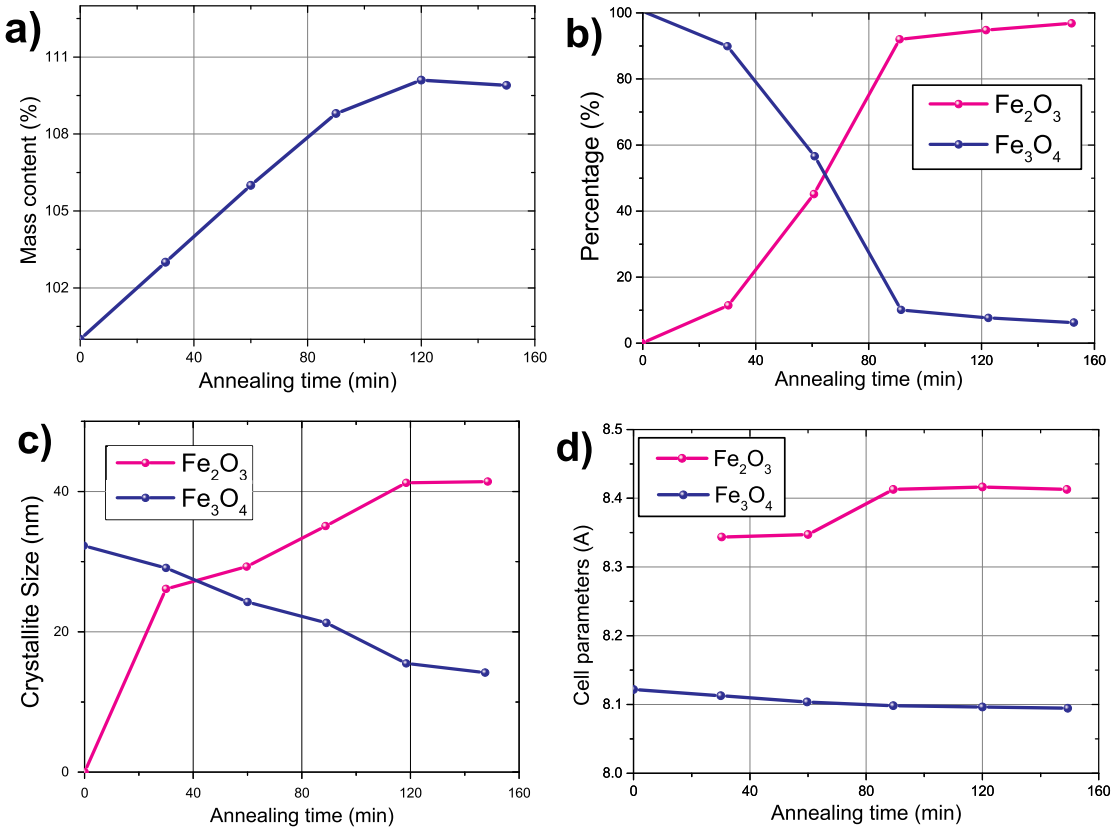

Figure 8. (a) Dependency graph of changing the sample mass during annealing; (b) diagram of phase transitions as a function of the annealing time; (c) dependency graph of the average crystallite size as a function of the annealing time; and (d) dependency graph of changing the cell parameter as a function of the annealing time.

Analysis of the oxidized samples

Figure 6 shows the dynamics of the surface morphology of magnetite powder depending on the duration of annealing time at a temperature of 300°C according to SEM data. The SEM images of Fe_3O_4 (magnetite) powder annealed at 300°C reveal gradual changes in surface morphology over time. Figure 6 also shows that longer heat treatment times for Fe_3O_4 phase gradually changes the morphology of the sample. After 30 and 60 min, minimal morphological changes occur in the form of coalescence. The magnetite phase remains stable during this time. At 90 min of annealing, surface changes become more noticeable. There is increased sintering, particle flattening and more porosity. XRD analysis indicates that after 65 min at 300°C, the maghemite phase (γ-Fe_2O_3) becomes dominant over the magnetite phase (Fe_3O_4). With continued annealing from 120 to 150 min, grain growth increases. Porosity becomes more pronounced, and the surface of the sample increases smoothness. At this stage, the phase transition to maghemite nears completion, leading to a denser and more stable microstructure. It was found that the crystallite size growth for the γ-Fe_2O_3 phase and the crystallite reduction for the Fe_3O_4 phase were observed with increasing the thermal treatment time. The magnetite-to-maghemite transition is accompanied by significant changes in surface texture and porosity, as well as an overall refinement of the material's morphology.

X-ray structural analysis (Figure 7) of magnetite Fe_3O_4 powders before their thermal annealing showed the presence of peaks characteristic of X-ray diffraction on polycrystalline objects. Figure 7 shows the evolution of XRD patterns corresponding to the samples subjected at different to thermal treatment time. The main phase is iron oxide Fe_3O_4 (space group Fd3 m) (PDF Card No. 261136). According to Equation (9), the value of the lattice parameter a is 8.121 Å, which exceeds the reference value of a = 8.090 Å.

Analysis of the obtained diffraction patterns has showed that the γ-Fe_2O_3 phase (space group $P4_132$) appears, and the phase transition process of the crystal structure from Fe_3O_4 to γ-Fe_2O_3 (PDF # 391346) with the preferred orientation of crystallites for the γ-Fe_2O_3 phase from the texture plane with Miller indexes (220) is observed because of thermal treatment of the initial powder. Table 3 presents the results of EDA analysis of samples after thermal treatment.

Analysis of the obtained results has showed that a restructuring of the crystal structure associated with the oxidation process is observed with increasing the annealing time. Figure 8(a) demonstrates a plot of

changing the sample mass during annealing. The sample mass growth can be explained by the restructuring of the crystal structure and the change in phase states due to the structure oxidation. Figure 8(b) shows a graph of changing the percentage of phases in the powder structure.

Two sections are clearly distinguished for both phase states on the presented graph. The first section from 0 to 90 min of annealing is characterized by a sharp change in the phase state of the structure, which may be caused by the surface layer oxidation due to thermal annealing. The second section from 90 to 150 min of annealing is characteristic for a slight change in the structure, which is explained by the slow oxidation of the internal structure of the hollow microsphere, due to the lack of full oxygen access into the spheres. Figures 8(c) and (d) show the results of changing the average size of crystallites during annealing, estimated from Equation (10) and changing the cell parameter as a function of the annealing time, respectively.

The crystallite size growth for the γ-Fe_2O_3 phase and the crystallite reduction for the Fe_3O_4 phase are observed with increasing the thermal treatment time. Changes in the crystallite size are associated with changing the lattice parameter *a*, which results are demonstrated in Figure 8(c). As can be seen from the data presented in Figure 8(c), the character of changes in the crystal lattice parameter is analogous to changes in the phase transitions shown in Figure 8(b). The annealing time growth after 90 min leads insignificant parameters change, which also confirms the earlier assumption that the oxidation process is slowing down during annealing due to the presence of an internal hollow structure, where oxygen access is limited, since oxides are formed predominantly on the sphere surfaces during the annealing process. Thus the controlled phase transition of Fe_3O_4 iron oxide into γ-Fe_2O_3 is presented by thermal treatment of Fe_3O_4 iron oxide in an oxygen-containing medium at a temperature of 300°C in the range from 30 to 150 min. The crystallite size of maghemite in this work is 42 nm (see Figure 8) and correlates well with those obtained elsewhere [18–20].

Conclusion

The thermal reduction and oxidation of iron oxide slags generated from rolling mill steel industry have been investigated. The composition of the rolled scale consists of wüstite, magnetite and hematite, with small impurities of manganese and aluminum which quantitative values decrease during the synthesis of hematite.

It is evident that iron oxides are formed because of the interaction of the rolled sheet with oxygen. A small part of iron is transferred to scale during mechanical cleaning of the sheet surface after rolling. The carbon-containing phase appears to be a product of the interaction of iron oxides with the oil used for rolling.

The initial scale particles were flake or lamellar in shape with particle sizes ranging from a few millimeters to several centimeters. The particle size varies from 200 nm to 150 μm. The sample is dominated by particles with flat faces with sharp angles. There are also particles with a shape close to spherical, 2–10 μm in size.

In addition, the controlled phase transition of Fe_3O_4 iron oxide to γ-Fe_2O_3 by heat treatment of Fe_3O_4 iron oxide in an oxygen-containing medium at 300°C for 30–150 min has been experimentally demonstrated. During the heat treatment in oxygen-containing medium, γ-Fe_2O_3 phases were formed and a phase transition of the crystal structure from Fe_3O_4 to γ-Fe_2O_3 with preferential crystallite orientation for the γ-Fe_2O_3 phase from the Miller index texture plane (220). It was found that with increasing heat treatment time, an increase in crystallite size for the γ-Fe_2O_3 phase and a decrease in crystallite size for the Fe_3O_4 phase were observed.

Acknowledgements

The authors express their gratitude to Arbuz A.S, Research Facility Coordinator from the Nazarbayev University, Kazakhstan., for assistance in conducting electron microscopic studies.

Disclosure statement

No potential conflict of interest was reported by the author(s).

Funding

J. Kargin acknowledges support from the JSC "Center for International Programs" of the Republic of Kazakhstan under the International Programme "500 scientists", Agreement for Scientific Internship No. 7971 dated July 18, 2023. H. Sanchez thanks the Peruvian Agency CONCYTEC for financial support through grant number PE501087367-2024-PROCIENCIA. The work in Brazil has been supported by the PROFESSOR VISITANTE Program No. 13/2022 of the Universidade Federal de Pernambuco, Brazil, Contract No. 0037 /2024 (Process no. 019063/2023-39) and CNPQ. The work in Barranca, Peru has been supported by a collaboration agreement between the National University of Barranca and the University of Cambridge (Contract No. RG92973).

Contribution statement

Data acquisition, methodology, data curation and formal analysis (J. Kargin, H.E Sanchez Cornejo, Y.V. Konyukhov, A.S. Lileev and A. Kozlovskiy), conceptualization, interpretation, validation, data curation and visualization (S.R. Celis Rojas, J. Albino Aguiar, V.A.J.

Silva, C.H.W. Barnes and L. De Los Santos Valladares) and all authors have contributed in writing the manuscript.

ORCID

L. De Los Santos Valladares http://orcid.org/0000-0001-5930-9916

References

[1] Ruhiyuddin MZ, Murizam D, Ahmad KR. Synthesis and characterization of iron produced from iron mill scale. Key Eng Mater. 2014;594–595:118–122. doi:10.4028/www.scientific.net/KEM.594-595.118

[2] Prim SR, Folgueras MV, de Lima MA, et al. Synthesis and characterization of hematite pigment obtained from a steel waste industry. J Hazard Mater. 2011;192:1307–1313. doi:10.1016/j.jhazmat.2011.06.034

[3] Carlini R, Alfieri I, Zanicchi G, et al. Synthesis and characterization of Iron-rich glass ceramic materials: a model for steel industry waste reuse. J Mater Sci Technol. 2016;32:1105–1110. doi:10.1016/j.jmst.2016.09.008

[4] Kargin J, De Los Santos Valladares L, Borja-Castro LE, et al. Characterization of iron oxide waste scales obtained by rolling mill steel industry. Hyperfine Interact. 2022;243:14. doi:10.1007/s10751-022-01800-7

[5] Bustamante Dominguez AG, Valerio-Cuadros MI, Borja-Castro LE, et al. Characterization and Mössbauer spectroscopy of steel slag generated in the ladle furnace in SIDERPERU steel plant. Hyperfine Interact. 2022;243:12. doi:10.1007/s10751-022-01799-x

[6] Valerio-Cuadros MI, Bustamante Domínguez AG, Valencia-Bedregal RA, et al. Structural and hyperfine magnetic properties of primary steelmaking slag. Hyperfine Interact. 2022;243:11. doi:10.1007/s10751-022-01797-z

[7] Cabrera-Tinoco HA, Valencia-Bedregal RA, Borja-Castro LE, et al. Characterization of black slags obtained during smelting in the electric arc furnace from SIDERPERU following reduction. Hyperfine Interact. 2022;243:8. doi:10.1007/s10751-022-01791-5

[8] Bhatta G, De Los Santos Valladares L, Bustamante Dominguez A, et al. Microstructure and tensile properties of fine-grained bulk copper fabricated by thermo-mechanical consolidation of copper nanopowder/micron-sized powder blend. Mater Res. 2022;25:e20210186. doi:10.1590/1980-5373-mr-2021-0186

[9] Suarez E, Borja-Castro SM, Valerio-Cuadros LE, et al. Carbothermal reduction of mil scales formed on steel billets during continuous casting. Hyperfine Interact. 2021;242:29. doi:10.1007/s10751-021-01769-9

[10] De Los Santos Valladares L, Battha G, Liu X, et al. Microstructure and mechanical properties of solid state recycled 4Cr5MoSiV (H11) steel prepared by powder metallurgy. Results Mater. 2021;10:100184. doi:10.1016/j.rinma.2021.100184

[11] Borja-Castro LE, Bustamante Dominguez A, Valerio-Cuadros MI, et al. Characterization of Steel billet scales generated during the continuous casting process in SIDERPERU steel plant. Hyperfine Interact. 2021;242:53. doi:10.1007/s10751-021-01778-8

[12] De Los Santos Valladares L, Bustamante Domínguez A, León Félix L, et al. Characterization and magnetic properties of hollow α-Fe_2O_3 microspheres obtained by sol gel and spray roasting methods. J Sci Adv Mater Dev. 2019;4:483–491. doi:10.1016/j.jsamd.2019.07.004

[13] De los Santos Valladares L, Mukhambetov DG, et al. Influence of space charge during the oxidation of metal surfaces. Oxid Met. 2018;90:515–526. doi:10.1007/s11085-018-9843-8

[14] De los Santos Valladares L, León Félix L, Coaquira JAH, et al. Structural and magnetic properties of core-shell Au/Fe_3O_4 nanoparticles. Sci Rep. 2017;7:41732. doi:10.1038/srep41732

[15] Zhang Y, Meng L, Zhao X, et al. The effects of extrusion ratio and heat treatment on microstructures and tensile properties of a powder metallurgy Fe-22Mn steel. Mater Sci Eng A. 2023;872:144944. doi:10.1016/j.msea.2023.144944

[16] Suer J, Traverso M, Jäger N. Review of life cycle assessments for steel and environmental analysis of future steel production scenarios. Sustainability. 2022;14(21):14131. doi:10.3390/su142114131

[17] De Los Santos Valladares L, León Félix L, Espinoza Suarez SM, et al. Preparation and crystallization of hollow (α-Fe_2O_3) microspheres following the gas-bubble template method. Mater Chem Phys. 2016;169:21–27. doi:10.1016/j.matchemphys.2015.11.021

[18] Lileev AS, Kargin J, Konyukhov YV, et al. The effects of thermomagnetic treatments on the magnetic properties of nanocrystalline Fe–O and Fe–O–O pressed compacts. J Supercond Novel Magn. 2025;38:8. doi:10.1007/s10948-024-06837-z

[19] Shilova OA, Nikolaev AM, Kovalenko AS, et al. Synthesis of magnetic nanopowders of iron oxide: magnetite and maghemite. Russ J Inorg Chem. 2020;65:426–430. doi:10.1134/S0036023620030134

[20] Biswas B, Lutfor Rahman M, Farid Ahmed M, et al. Extraction of gamma iron oxide (γ-Fe_2O_3) nanoparticles from waste can: structure, morphology and magnetic properties. Heliyon. 2024;10:e30810. doi:10.1016/j.heliyon.2024.e30810

[21] Santos LGD, Buelvas DDA, Valezi DF, et al. Microstructural and magnetic properties of polyamide-based recycled composites with iron oxide nanoparticles. Magnetism. 2025;5(1):5. doi:10.3390/magnetism5010005

[22] Khanna R, Konyukhov Y, Li K, et al. Innovative transformation and valorisation of Red Mill Scale waste into ferroalloys: carbothermic reduction in the presence of alumina. Sustainability. 2023;15(24):16810. doi:10.3390/su152416810

[23] Tolstoi VP. Synthesis of thin-layer structures by the ionic layer deposition method. Russ Chem Rev. 1993;62(3):237. doi:10.1070/RC1993v062n03ABEH000015

[24] Klimov VI, Bolívar PH, Kurz H, et al. Linear and nonlinear transmission of CuxS quantum dots. Appl Phys Lett. 1995;67(5):653–655. doi:10.1063/1.115192

[25] León L, Bustamante DominguezOsorio A, Olarte AG, et al. Synthesis and characterization of hollow (α−Fe_2O_3) submicron spheres prepared by sol–gel. Hyperfine Interact. 2011;202:131–137. doi:10.1007/s10751-011-0353-1

[26] De Los Santos Valladares L, León Félix L, Espinoza Suarez SM, et al. Preparation and crystallization of hollow (α-Fe_2O_3) microspheres following the gas-bubble template method. Mater Chem Phys. 2016;169:21–27. doi:10.1016/j.matchemphys.2015.11.021

[27] Opila EJ. High temperature materials corrosion challenges for energy conversion technologies.

Electrochem Soc Interface. 2013;22(4):69–73. doi:10.1149/2.F07134if

[28] Kozlovskyi AL, Kargin JB, Kokarev MZ, et al. Study of the iron nanoparticles phase transformation during thermal annealing. Chem Bull Kaz Nat Univ. 2017;1(84):16–25. doi:10.15328/cb796

[29] Schiemann M, Wirtz S, Scherer V, et al. Spray roasting of iron chloride $FeCl_2$: laboratory scale experiments and a model for numerical simulation. Powder Technol. 2012;228:301–308. doi:10.1016/j.powtec.2012.05.037

[30] Wang L, Lu X, Han C, et al. Electrospun hollow cage-like α-Fe_2O_3 microspheres: synthesis, formation mechanism, and morphology-preserved conversion to Fe nanostructures. CrystEngComm. 2014;16:10618–10623. doi:10.1039/C4CE01485E

[31] Li L, Chu Y, Liu Y, et al. Template-free synthesis and photocatalytic properties of novel Fe_2O_3 hollow spheres. J Phys Chem C. 2007;111(5):2123–2127. doi:10.1021/jp066664y

[32] De Los Santos Valladares L, Bustamante Domínguez A, León Félix L, et al. Characterization and magnetic properties of hollow α-Fe_2O_3 microspheres obtained by sol gel and spray roasting methods. J Sci Adv Mater Dev. 2019;4:483–491. doi:10.1016/j.jsamd.2019.07.004

[33] Konyukhov YV, Nguyen VM, Ryzhonkov DI. Kinetics of reduction of α-Fe_2O_3 nanopowder with hydrogen under power mechanical treatment in an electromagnetic field. Inorg Mater Appl Res. 2019;10(3):706–712. doi:10.1134/S2075113319030171

[34] Konyukhov YV, Ryzhonkov DI, Levina VV, et al. Producing iron nanopowders from iron ore. Steel Transl. 2005;35(3):17–21.

[35] Hechavarría R, López G. Fundamentals of steelmaking by E. T. Turkdogan. J Chem Inf Model. 2013;53:1689–1699. doi:10.1017/CBO9781107415324.004

[36] Taylor A, Sinclair H. Proc Phys Soc. 1945;57:126. doi:10.1088/0959-5309/57/2/306

[37] Nelson JB, Riley DP. An experimental investigation of extrapolation methods in the derivation of accurate unit-cell dimensions of crystals. Proc Phys Soc. 1945;57:160–177. doi:10.1088/0959-5309/57/3/302